Journal of Marine Science and Application (2026) 25: 32-45
https://doi.org/10.1007/s11804-025-00686-5

RESEARCH ARTICLE

Study on the Motion Characteristics of Floating Bubbles near the Wall Based on OpenFOAM

Jie Cui[1], Tao Xia[1], Zhaoyu Qu[1], Xin Chen[2] and Mingyuan Li[1]

Received: 28 October 2024 / Accepted: 22 January 2025

Abstract

In this study, the dynamic characteristics of microscale floating bubbles near the vertical wall are studied. This occurrence is common in industrial and natural phenomena. Although many studies have been conducted on microscale bubbles, few studies investigate floating bubbles with very small Reynolds number (*Re*) near the wall, which is the main research goal of this study. Therefore, this study establishes a model for the ascent of small-scale bubbles near a vertical wall using the interFoam solver in OpenFOAM. This study investigates the influences of diverse viscosity parameters, varying distances from the wall, and different gas flow rates on the terminal velocity, deformation, and motion trajectory of bubbles. The results reveal that as liquid viscosity increases, the *Re* of bubbles gradually decreases and reaches a minimum of 0.012, which is similar to the *Re* of micrometer-sized bubbles in water. The characteristics of the wall-induced force in the longitudinal direction are closely related to the changes in liquid viscosity. Under low-viscosity conditions, the induced lift is the principal form of action, whereas under high-viscosity conditions, it is primarily manifested as induced drag.

Keywords Rising bubble; Viscosity; Low Reynolds number; Near wall bubbles; OpenFOAM

1 Introduction

The dynamic evolution of small-scale microbubbles near the vertical wall is of great importance in numerous fields, including heat transfer, chemical engineering, microfluidic technology, and biotechnology. These applications utilize the ability of microbubbles to enhance mass and heat transfer, reduce resistance, and manipulate fluid flow, which is crucial for improving the efficiency and effectiveness of various industrial and scientific processes. The Reynolds number (*Re*) of these microbubbles is very low, between 0 and 10. However, most of the current research on microbubbles focuses on *Re* between 10 and $O(10^3)$. Thus, conducting basic research on floating microbubbles with *Re* = 0–10 is very important. At present, research methods such as theoretical analysis, experimental measurement, and numerical simulation are employed to study the velocity, deformation, rupture, and fusion characteristics of bubble floating. Corchero et al. (2006) experimentally examined the generation of bubbles by injecting a constant flow of air into an orifice immersed in water. Holes with different radii, including hydrophilicity and hydrophobicity, were drilled on horizontal plates of different materials to cover a series of static contact angles, and a wide range of volumetric gas flow rates were analyzed. The results show that the data of different static contact angles and orifice radii can be approximately simplified to a single bubble volume/flow association when the relationship between the appropriate proportion of detached bubble volume and the appropriate proportion of gas volume flow is drawn. Gong et al. (2020) constructed a visual bubble observation platform with an adjustable wall surface and observed the influence of wall surface with different inclination angles and wettability on bubble rising behavior. During the experiment, the velocity vector field of water around the rising bubble was obtained by particle image velocimetry. Through experiments, the instantaneous rising velocity, average rising velocity, and flow field around the bubble under different conditions were obtained, and the morphological changes of the bubble during rising were found. Takemura et al.

Article Highlights

- The motion characteristics of bubbles near the wall are studied using a combination of experimental and numerical methods.
- A small hole bubble model near the wall is proposed.
- The effects of different viscosities, distance parameters, and gas flow rates on bubble motion characteristics are investigated.

✉ Zhaoyu Qu
quzhaoyu@just.edu.cn

[1] School of Naval & Ocean Engineering, Jiangsu University of Science and Technology, Zhenjiang 212100, China

[2] School of Materials Science and Engineering, Jiangsu University of Science and Technology, Zhenjiang 212100, China

(2002) experimentally measured the two components of the force acting on a clean near-spherical bubble rising on a near-plane vertical wall in a static liquid. A charge-coupled device (CCD) camera and a microscope were used to follow the rising bubbles. The device can accurately measure the radius of the bubble, the rising speed, and the distance between the bubble and the wall. Thus, the resistance and lift components of the hydrodynamic force are determined when *Re* (based on bubble diameter, rising velocity *U*, and kinematic viscosity *v*) is less than 40. Tian et al. (2019) experimentally examined the shape and rising velocity of bubbles in silicone oil and paraffin under the influence of high temperature and high pressure and proposed a new correlation of bubble aspect ratio. Rozario et al. (2018) used water and oil to represent liquid metal and slag, respectively. They simulated the bubble rising through the interface layer of molten metal and slag through experiments and concluded that the interface between the two liquid layers reaches a quasi-stationary state in a certain period. Shi et al. (2023) experimentally investigated the dynamic characteristics of submillimeter bubbles rising in inclined laminar channel water with a bubble *Re* of approximately 100. Zheng et al. (2023) experimentally studied the rising of single CO_2 bubbles in a monoethanolamine solution. The results are of great importance for the mass transfer in gas–liquid reaction flow and the design of a multiphase reactor. Jeong and Park (2015) experimentally analyzed the near-wall rising behavior of deformable bubbles at high Reynolds numbers ($Re \sim O(10^3)$). Takemura and Magnaudet (2003) studied the interaction between the bubble and the wall at *Re* calculated from the floating velocity and the equivalent radius. When *Re* is small, the bubble stays away from the wall when it floats because the repulsive force generated by the wall is combined with the repulsive force of vorticity diffusion (Takemura et al., 2002). When *Re* increases, the vorticity generated by the bubble is retained in the bubble boundary layer. The liquid velocity between the bubble and the wall is small and results in an uneven velocity distribution around the bubble. According to potential flow theory, the uneven velocity distribution generates a pressure gradient, which causes the bubble to migrate to the wall. However, when the bubble moves to the wall, the distance between the bubble and the wall decreases (Sugiyama and Takemura, 2010). Due to the influence of the viscosity of the thin liquid layer between the bubble and the wall, i.e., lubrication theory, the force on the bubble changes the direction so that the bubble begins to move in the opposite direction. Snabre and Magnifotcham (1998) considered the continuous emission of bubbles from a single jet hole immersed in a viscous fluid. First, a semiempirical model for the growth of spherical bubbles under constant flow conditions was given to predict the bubble volume in the detachment stage. Then, a physical model was proposed to describe the rising velocity of the online interacting bubbles, and the expression of the net viscous force acting on the surrounding fluid was derived. The experimental results of an air/water–glycerol system in a wide range of fluid viscosity (43–800 mPa·s) were presented and compared with the theoretical prediction. An imaging technique was used to determine the size and rising velocity of bubbles. The effects of fluid viscosity, gas flow rate, orifice diameter, and liquid depth on bubbles were examined. Zhang et al. (2008) measured the unsteady motion of a single bubble rising freely in a high-viscosity static liquid using a CCD camera. Image analysis software was used to digitize and examine the recorded frame sequence, and the measured values of the acceleration and steady-state motion of the bubble were obtained. The total resistance coefficient from accelerated motion to steady-state motion was calculated, including additional mass force and historical force. Dimensional analysis, based on the equivalent bubble diameter, revealed that the total drag coefficient of a single bubble is a function of acceleration number, Archimedes number, and *Re*.

In numerical simulation, commonly used computational methods include the finite element method, finite volume method, boundary element method, SPH method. Gan et al. (2022) studied the situation of gas injection from the surface of a vertical plate based on OpenFOAM and examined the cross-flow of ventilated bubble injection. Then, the effects of contact angle, incoming flow direction relative to gravity, and surface tension on the dynamic behavior of ventilated bubbles were analyzed. Amaya-Bower and Lee (2010) investigated the dynamic behavior of a single rising bubble by using the lattice Boltzmann method based on the Cahn–Hilliard diffusion interface method. The bubble rises due to gravity. However, the deformation and velocity of bubbles depend on the balance of other forces generated by surface tension, inertia, and viscosity. According to the primary force acting on the system, bubble dynamics can be split into different regimes. Based on open-source software Basilisk, Yan et al. (2023) numerically simulated a single bubble floating near the vertical wall and examined various types of bubble migration paths, such as linear, serrated, and spiral. Xu et al. (2023) simulated the bubble rising in viscous static liquid based on the incompressible smoothed particle hydrodynamics and finite volume method coupling method and confirmed the accuracy and stability of the coupling model. Naseer et al. (2023) investigated the interaction of two parallel bubbles rising in a static viscoelastic fluid under a series of parameters by using the 3D interface-resolved numerical simulation method. The effects of the shape, velocity, and interaction of the two bubbles were analyzed in detail. Debisschop et al. (2000) explored the dynamics of bubble rising in a 2D inclined channel. The fluid obeys the Stokes equation, and the boundary integral method is used to solve the bubble dynamics. Consider bubbles containing insoluble sur-

factants and bubbles without insoluble surfactants. The bubble dynamics under different inclination angles, Bond numbers, and other physical parameters were studied. When the Bond number is large enough, a liquid line is formed on the bubble interface. For a sufficiently large inclination angle, the bubble may bounce along the top wall of the channel. Premlata et al. (2015) numerically studied bubble rising dynamics in a static, unconstrained, viscous layered medium. The results show that in a medium with a linear increase in viscosity, at a certain parameter value, the bubbles undergo large deformation by forming a slender skirt, and the skirt physically separates the wake region from the rest of the surrounding fluid. This special dynamics is attributed to the migration of low-viscosity fluids. When the bubble rises, these fluids are carried in the bubble wake and lead to an increasing viscosity contrast between the fluid in the wake region and the surrounding fluid, which is different from what is observed in a constant-viscosity medium. Mundhra et al. (2023) performed a 3D numerical simulation based on the volume of fluid (VOF) method. The effects of wall proximity and surface tension on bubble trajectory were studied. Zhang et al. (2024) established a theoretical model of bubble dynamics that considers factors such as liquid compressibility, phase change, oscillation, migration, and environmental flow field. The theoretical model effectively captures the experimental results of bubbles generated in the free field, near the free surface, near the rigid wall, and near other bubbles. Based on existing theory, the influence of bubble content on the initial high-pressure bubble is discussed by changing the proportion of steam in the initial high-pressure cavitation bubble.

Previous studies have mainly focused on the near-wall rising dynamics of bubbles at higher Eotvos numbers (Eo) and different Galilei numbers (Ga). The physical properties of the flow are selected so that the freely rising bubbles are in a straight line. The number of Ga is fixed, and the number of Eo is changed to analyze its influence on the bubble's rising trajectory. The presence of the wall increases the resistance of the bubble and induces the early transition of the bubble from a straight line to a plane zigzag. The maximum wall distance and critical Eo number of bubbles moving along the bouncing trajectory are determined. The amplitude, frequency and wavelength of the bounce motion are independent of the initial wall distance but decrease with the decrease of the surface tension. At present, the application of computer technology in the field of bubble floating has matured. However, due to the small bubble size, unstable deformation and multimedia, multi-bubble interaction, the calculation accuracy and calculation time are difficult to guarantee. In terms of experiments, at present, bubbles are primarily discharged into the liquid through pinholes or air compressors and combined with high-speed photography technology for research. However, microbubbles are difficult to generate through experiments due to their small size. Therefore, numerical simulation is the most effective method for studying microbubbles with low *Re*.

To address the above problems, a 2D model of floating bubbles near the wall is established in this study based on the interFoam solver in open-source software OpenFOAM, and the numerical method is verified by model tests. The variation of the final floating velocity, deformation, and trajectory of the bubble under the influence of different distances from the wall and dissimilar gas flow rates in different viscous media is studied. This study provides an effective theoretical and technical basis for industrial, chemical, and cleaning fields.

2 Numerical method

In the study of bubble dynamics, the ability to describe the motion interface of gas–liquid two-phase flow accurately and stably is an important factor in investigating the change of bubble motion. Because the VOF method tracks the fluid volume in the grid, it does not track the movement of fluid particles. The VOF method has the advantages of easy implementation, small amount of calculation, and high precision. Therefore, this paper uses the interFoam solver in OpenFOAM to perform 2D numerical simulation and constructs the gas–liquid interface based on the VOF model.

2.1 Free surface tracking method

The VOF method is used to track the gas–liquid interface. The basic principle is to determine the position and shape of the free surface by calculating the volume ratio function of the fluid and the grid unit in the grid unit. The phase fraction of the fluid is represented by defining variable α, as presented in Figure 1.

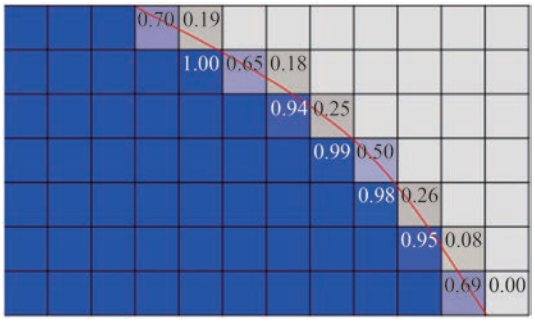

Figure 1 Gas–liquid two-phase phase fraction diagram of grid unit

$$\begin{cases} \alpha = 0, & \text{air} \\ \alpha = 1, & \text{fluid} \\ 0 < \alpha < 1, & \text{two-phase flow} \end{cases} \tag{1}$$

When $\alpha = 1$, the grid unit is liquid phase; when $\alpha = 0$, the grid unit is gas phase. The gas–liquid interface can be positioned as α between 0 and 1.

The gas–liquid interface can be solved by the following equations:

$$\frac{\partial \alpha}{\partial t} + \nabla \cdot (\alpha \boldsymbol{u}) = 0 \tag{2}$$

where α is the phase fraction parameter, $\boldsymbol{u}$ is the common velocity vector of the two fluids in the whole basin, and t is the time.

Density ρ and viscosity μ are weighted by phase fraction as follows:

$$\rho = \alpha \rho_l + (1 - \alpha)\rho_g \tag{3}$$

$$\mu = \alpha \mu_l + (1 - \alpha)\mu_g \tag{4}$$

where l and g are the liquid phase and gas phase, respectively.

The continuous medium surface force model is used for surface tension. The surface tension is calculated as follows:

$$F_\sigma = \pi d \sigma \cos\theta \tag{5}$$

where σ is the surface tension coefficient, d is the inner diameter of the outlet, and θ is the angle between the vertical line and the bubble surface on the nozzle.

2.2 Governing equations

The VOF method involves the simultaneous solution of the continuity equation and momentum equation and the solution of the transport equation of the phase fraction.

The incompressible continuity equation is expressed as follows:

$$\nabla \cdot \boldsymbol{u} = 0 \tag{6}$$

The momentum equation is expressed as follows:

$$\frac{\partial \rho \boldsymbol{u}}{\partial t} + \nabla \cdot \left(\rho \boldsymbol{u}\boldsymbol{u}\right) = -\nabla p + \nabla \cdot \left[\mu\left(\nabla \boldsymbol{u} + \nabla \boldsymbol{u}^{\mathrm{T}}\right)\right] + \boldsymbol{F}_\sigma + \rho \boldsymbol{g} \tag{7}$$

where p is the static pressure, $\boldsymbol{F}_\sigma$ is the surface tension, and μ is the liquid viscosity. In a single-pressure system, on a fixed nonvertical nonslip solid wall, due to the existence of the fluid static component $\rho \boldsymbol{g}$ when the two phases are separated on the wall, the normal components of the pressure gradient of each phase must be different.

To simplify the definition of boundary conditions, correction pressure is defined as follows:

$$p_d = p - \rho \boldsymbol{g} \cdot \boldsymbol{x} \tag{8}$$

where $\boldsymbol{x}$ is the position vector of the fluid element.

The momentum modified by Eq. (8) is expressed as follows:

$$\frac{\partial \rho \boldsymbol{u}}{\partial t} + \nabla \cdot \left(\rho \boldsymbol{u}\right) = -\nabla p_d - \boldsymbol{g} \cdot \boldsymbol{x} \nabla \rho + \nabla \cdot \left[\mu\left(\nabla \boldsymbol{u} + \nabla \boldsymbol{u}^{\mathrm{T}}\right)\right] + \boldsymbol{F}_\sigma \tag{9}$$

2.3 Bubble size and volume

As shown in Figure 2, the bubbles generated at a small flow rate are only affected by buoyancy and surface tension, and the effects of viscous force and inertial force are ignored. Buoyancy is expressed as follows:

$$\boldsymbol{F}_f = \left(\rho_l - \rho_g\right) V_b \boldsymbol{g} \tag{10}$$

where V_b is the volume when the bubble is generated, which can be calculated according to $V_b = \pi d_b^3/6$, d_b is the diameter of the bubble when it leaves the outlet.

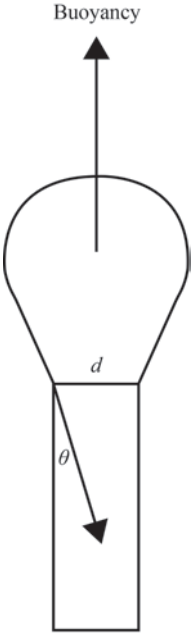

Figure 2 Force and size of bubble formation

When the bubble separates from the outlet, the force of the bubble reaches equilibrium:

$$\boldsymbol{F}_f = \boldsymbol{F}_\sigma \tag{11}$$

The theoretical formula of bubble departure diameter can be obtained by substituting Eqs. (5) and (10) into Eq. (11). To facilitate the calculation, let $\theta = 0$, then $\cos\theta = 1$:

$$d_b = \left[\frac{6\sigma d}{\left(\rho_l - \rho_g\right) g}\right]^{\frac{1}{3}} \tag{12}$$

When dimensionless calculation is involved, the initial radius R of the bubble just leaving the outlet is selected as the length factor, and the initial radius R can be solved by Eq. (12):

$$R = \frac{d_b}{2} \tag{13}$$

Bubble Re is expressed as follows:

$$Re = \frac{\rho_l V_T d_b}{\mu_l} \tag{14}$$

where ρ_l is the liquid density, V_T is the bubble terminal velocity, d_b is the bubble diameter, and μ_l is the dynamic viscosity of the liquid phase.

2.4 Bubble-wall interaction

In this study, the research on the dynamic characteristics of microscale bubbles near the vertical wall is equivalent to ignoring the motion of microscale bubbles on the vertical plate under the action of gravity. The bubble motion induces a laminar boundary layer near the wall. The thickness of the laminar boundary layer on the plate is expressed as follows:

$$\delta \propto \frac{x}{\sqrt{Re}} \tag{15}$$

where δ is the boundary layer thickness, and x is the distance along the plate.

The shear stress on the bubble surface in the laminar boundary layer is expressed as follows:

$$\tau = \mu \frac{\mathrm{d}u}{\mathrm{d}x} \tag{16}$$

where τ is the shear stress, and $\frac{\mathrm{d}u}{\mathrm{d}x}$ is the velocity gradient perpendicular to the wall.

3 Numerical method validation

3.1 Experimental method

Figure 3 is the schematic diagram of the floating bubble test device. The test was completed in an open water tank. The water tank is 200 mm high, and the bottom is a square with a side length of 100 mm. The water tank and the movable wall are made of high-strength acrylic light-transmitting plate, and the side of the wall is black-marked for easy observation. The high-speed camera is VRI-PhantomV611, and 10 000 images are collected per second for 6 seconds. The light source is a flat-panel fill light, and the backlight is used to observe the bubble shape change and trajectory. The bubble generator uses a high-precision syringe, which can accurately control the flow of air to guarantee the accuracy of the experiment.

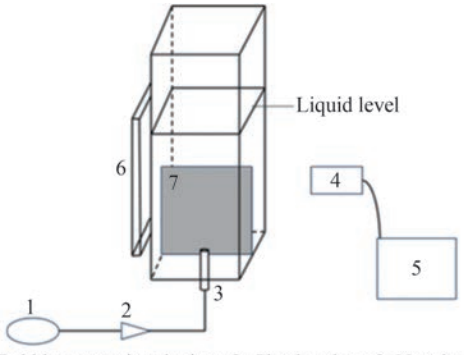

1. Bubble generating device; 2. Check valve; 3. Nozzle;
4. High-speed camera; 5. The computer connected to the camera;
6. Flat fill light; 7. Vertical movable wall

Figure 3 Diagram of experimental device

3.2 Geometric model and boundary conditions

Considering that many factors affect the movement of microbubbles in the process of rising near the vertical wall, to make the research universal, a 2D vertical wall model is established in this paper to study the influence of liquid viscosity, the distance between the bubble and the wall, and the gas flow rate on its movement.

A 2D numerical model of floating bubbles near the wall is established based on the VOF method, as shown in Figure 4. The Euler domain is 45 mm long and 160 mm high. The bubble is generated by an outlet with a diameter of 3 mm, and the height from the outlet to the bottom of the Euler domain is H = 30 mm. The Euler domain contains only three materials: air, silicone oil, and rigid wall. The outlet is set as the velocity inlet, the velocity is set to 0.001 m/s, the interface between air and silicone oil is set as the pressure outlet, the wall slip condition is nonslip, and the contact angle is 45°. The fluid material is incompressible fluid, and the flow state is laminar flow and transient flow.

3.3 Validation of VOF method

Figure 5 compares the model experiment and numerical simulation of silicone oil with bubble–wall distance parameter λ = 1 and liquid viscosity of 100 cs (1 cs = 10^{-6} m^2/s) (Re = 4). Because of the high-viscosity silicone oil used in this paper, the equivalent diameter of the bubble is approximately 4 mm, and the Re is between 0 and 5, which is similar to the Re of the microbubble. The upper set of views (a) is the floating bubble experiment near the wall, and the lower set of attempts (b) is the numerical simulation results. The bubble floating time is marked in the upper left of each frame of the picture, and the unit is ms.

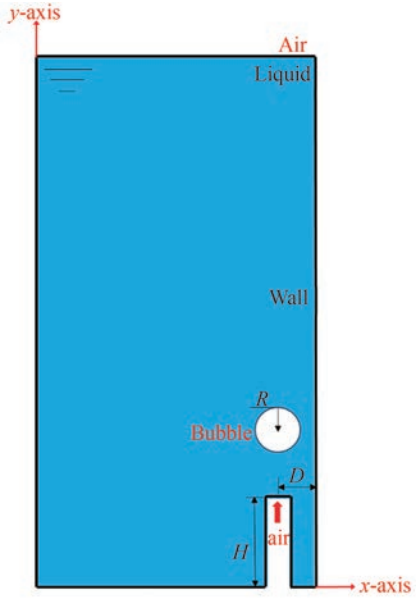

Figure 4 Geometric model of bubble formation and rising

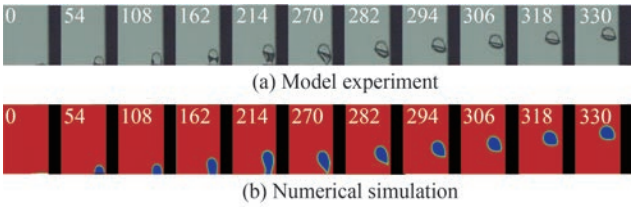

Figure 5 Comparison of bubble morphology in silicone oil with distance parameter $\lambda = 1$ and viscosity 100 cs ($Re = 4$)

The figure shows the change of bubbles from the generation stage to the stable floating stage. The bubble morphology of the numerical simulation agrees with that of the bubble experiment in each stage. The time required in the bubble generation stage is longer than that of the bubble leaving the outlet to reach a stable state, so the time interval between the generation stage and the floating stage in the figure is different. In this study, the same outlet parameters as the experiment are used to study the influence of medium viscosity, wall distance parameters, and gas outlet velocity on the dynamic evolution characteristics of floating bubbles near the wall.

Figure 6 compares the numerical and experimental results of the final velocity and lateral and vertical displacement of bubbles near the wall. The numerical simulation results agree with the terminal velocity and displacement curves of the floating bubble experiment near the wall.

The initial radius of the bubble in the experiment is 4 mm when it is separated from the outlet. The radius of the numerical simulation is 3.8 mm, and the error is 5%; according to the volume calculation in Eq. (10), the error between the numerical value and the experimental bubble volume is 10.2%, and the maximum velocity error is 5.26%. Figure 6 compares the final floating velocity of the bubble and the

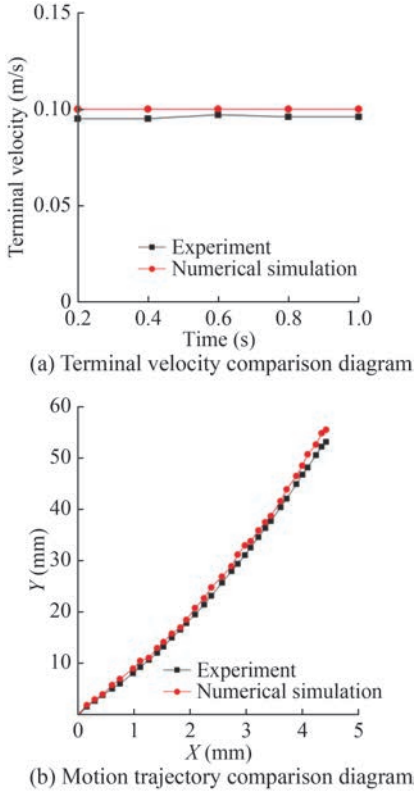

Figure 6 Comparison of bubble terminal velocity and motion trajectory

aspect ratio of the bubble and the test. The numerical calculation results agree with the model test, and the numerical method established in this paper has satisfactory accuracy.

3.4 Mesh convergence verification

The numerical simulation is discretized using a uniform grid to obtain the same level of accuracy in the whole computational domain. To verify the convergence of the model mesh, four different sizes of mesh elements are selected. These four grids are used to simulate the working condition of 1 times the bubble radius from the wall in 100 cs silicone oil. The bubble rising trajectory simulated by each size of the mesh is compared with the terminal velocity and the experimental results to obtain the optimal mesh unit size.

Table 1 Mesh scheme

Case	Mesh size (mm)	Mesh number
Case 1	0.1	699 000
Case 2	0.2	174 750
Case 3	0.4	43 800
Case 4	0.6	19 440

Figures 7 and 8 compare the mesh quality and gas–liquid interface under four mesh cell sizes. To observe the morphological changes of bubbles accurately during floating, the

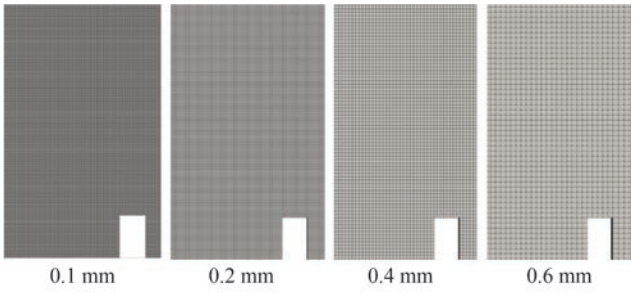

Figure 7 Comparison of four mesh sizes

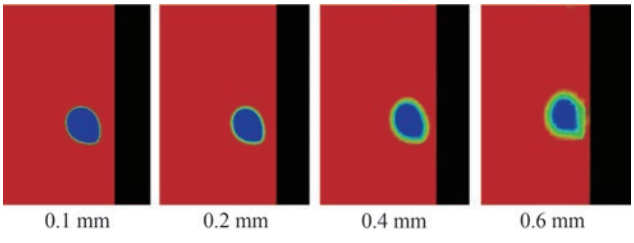

Figure 8 Gas–liquid interface of different mesh cell sizes

bubble surface must have a satisfactory resolution. Figure 7 shows that the mesh sizes of 0.4 and 0.6 mm are larger, and the outlet mesh is not dense enough. Figure 8 presents that the 0.1 and 0.2 mm mesh sizes can clearly show the bubble, whereas the 0.4 and 0.6 mm mesh size gas–liquid two-phase interface is blurred, and clearly analyzing the bubble deformation is difficult.

Figure 9 compares the terminal velocity and trajectory of the bubble under four mesh sizes with the experimental results. The velocity and trajectory obtained by 0.1 and 0.2 mm mesh sizes agree with the experimental results, and the error is approximately 5%. The larger the mesh size is, the faster the terminal velocity of the bubble is, and the trajectory is gradually messy. The calculation time of 0.1 mm mesh size is longer than that of 0.2 mm mesh size, and the efficiency is low.

In summary, the 0.2 mm mesh size agrees with the experimental results in the description of bubble morphology and the measured bubble velocity and trajectory, and the computational efficiency is high. Therefore, 0.2 mm can be used as the optimal mesh unit size for the calculation of the following conditions.

3.5 Time step independence verification

The selection of the time step also affects the accuracy and efficiency of the numerical solution. Based on mesh case 2, three groups of time steps are set, as shown in Table 2, and other settings remain unchanged to verify the independence of the calculated time step.

Figure 10 reveals that the time step slightly affects the final velocity and displacement of the bubble. The velocity and displacement calculated by Case 1 are the best with the experimental results, but the calculation time is long, and the efficiency is low, whereas the velocity calculated by

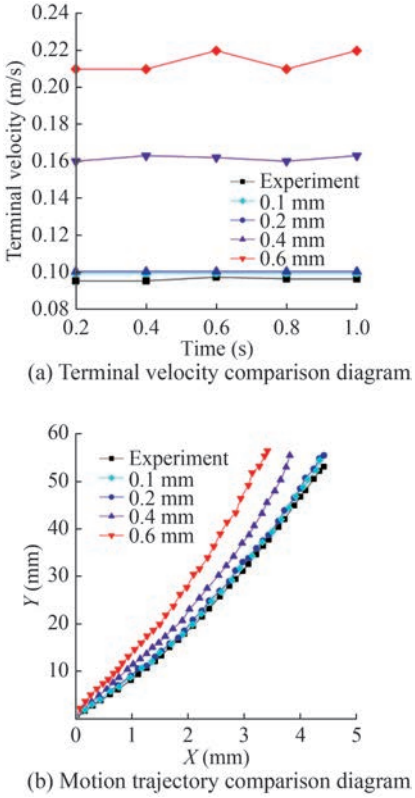

Figure 9 Comparison of bubble terminal velocity and trajectory changes with different mesh sizes

Table 2 Time step scheme

Case 1	Case 2	Case 3
4×10^{-5}	2×10^{-4}	1×10^{-3}

Case 3 has a slight error with the experiment. Considering the calculation cost and accuracy, the time step of 0.000 2 s in Case 2 is selected as the final calculation time step.

4 Results and discussions

4.1 Effect of liquid viscosity on the dynamic characteristics of floating bubbles

4.1.1 Research conditions

In this section, the effect of liquid viscosity on bubble motion is investigated. First, the bubbles in the free field of silicone oil with viscosity of 100, 500, and 1 000 cs are examined. Then, the bubbles near the wall in these three kinds of silicone oil are studied and compared with the experimental results. The experiment and the numerical values take the moment when the bubble just leaves the outlet as the initial moment, and the distance parameter between the bubble and the wall is $\lambda = 1$. The material parameters used in this paper are shown in Table 3, where v is the dynamic viscosity.

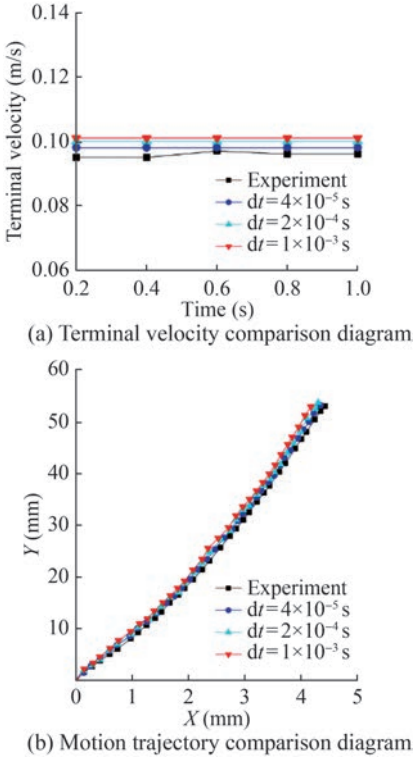

Figure 10 Comparison of bubble terminal velocity and trajectory changes with different time steps

Table 3 State parameters of each material

Silicon oil/Air	ρ (kg/m^3)	v (m^2/s)	σ (kg/s^2)
1 cs	816	10^{-6}	0.020
10 cs	935	10^{-5}	0.021
20 cs	949	2×10^{-5}	0.021
100 cs	964	10^{-4}	0.021
500 cs	970	5×10^{-4}	0.023
1 000 cs	971	10^{-3}	0.025
Air	1	1.48×10^{-4}	–

4.1.2 Bubble dynamics

For the bubbles floating in the free field, due to the combined effect of buoyancy and surface tension, the shape of the bubble at the initial stage presents an upper spherical shape and a lower conical shape. The local curvature at the bottom of the cone-shaped bubble is large, and the surface tension here is also large. Therefore, in the initial stage, the conical part of the lower part of the bubble bounces up rapidly, and the conical part of the lower end disappears rapidly and finally forms spherical, ellipsoidal, or irregular skirt-shaped bubbles.

Figure 11 shows the initial shape of bubbles near the free field and wall surface of low-viscosity silicone oil, where the number in the lower left corner of the picture is time, and the unit is ms. The bubbles generated in low-viscosity silicone oil are spherical at the top and conical at the bottom. After leaving the bubble mouth, the bottom of the cone shrinks rapidly and gradually becomes flat. As the bottom of the bubble further shrinks, the bubble becomes an approximately semicircular shape.

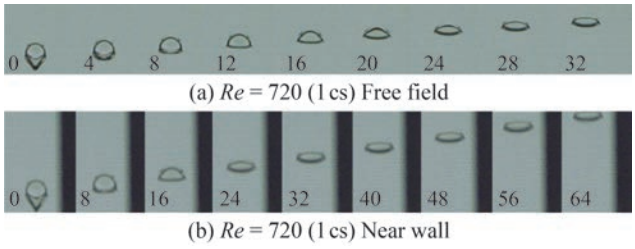

Figure 11 Comparison of initial bubble morphology in the free field and near wall of low-viscosity silicone oil

Next, this study focuses on the influence of different viscosity media on the dynamic characteristics of bubbles. Figure 12 compares the numerical and experimental changes of bubble morphology when floating in high-viscosity silicone oil. The left number in the figure is silicone oil with different viscosity parameters, and the lower left number is the image interception time in ms. For the morphological changes of floating bubbles in high-viscosity silicone oil, due to the increase of viscosity, the changes cannot be observed at the same time. Therefore, the morphological changes of bubbles in the three kinds of silicone oil intercepted in Figure 12 are different time distributions.

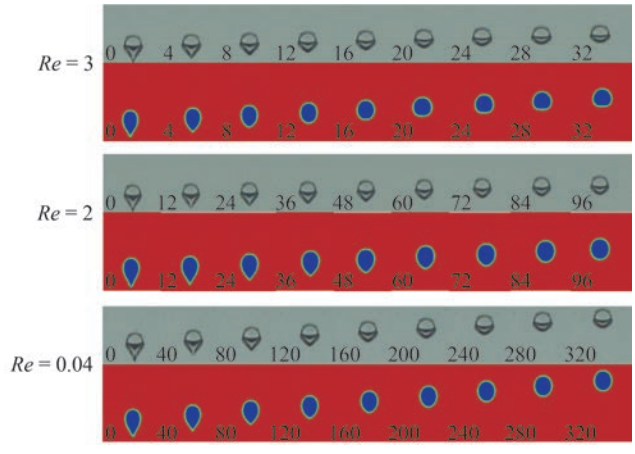

Figure 12 Comparison of initial bubble morphology in high-viscosity silicone oil free field

The three cases of Figure 12 are 100, 500, and 1 000 cs viscosity silicone oil bubble morphology changes. When the viscosity of silicone oil is in the range of 100–1 000 cs, *Re* decreases due to the increase of viscosity, and *Re* in 1 000 cs silicone oil is only 0.04. After the bubble separates from the outlet hole, although the bottom cone area also shrinks upward, it keeps the bottom cone and shrinks slowly,

and the shape of the upper half of the bubble remains unchanged. When the bottom is completely contracted, it is gradually rounded and reaches a stable state, and then it rises steadily. In general, the bubble deformation is very small. In 500 and 1 000 cs viscosity silicone oil, the stable state is very close to the circular bubble.

When the bubble approaches the solid surface, the shear stress of the fluid gradually increases. The velocity of the fluid near the wall generates a substantial gradient due to the viscous effect, which causes the bubble to produce local shear force when approaching the wall. This shear force typically concentrates on the surface of the bubble, especially near the wall. Under the action of high shear stress, the bubble undergoes asymmetric deformation. Near the wall, the fluid velocity is low, and the shear force on the bubble surface is strong, which may cause the bubble to flatten in the area near the wall, while the part away from the wall is subjected to small shear force, and the bubble shows a deformation in the direction of flow. For example, bubbles become elongated ellipsoids or hemispheres.

Figure 13 compares the initial morphological changes of floating bubbles near the wall surface in three kinds of high-viscosity silicone oil (100–1 000 cs). Due to the increase in viscosity, the changes cannot be observed at the same time, so the bubble morphology changes intercepted in Figure 13 are distributed at different times. With the increase of viscosity, the wall effect is considerably enhanced, which greatly influences the bubble formation stage. According to the calculation, the *Re* of bubbles is related to the viscosity of the liquid. The silicone oil with a viscosity of 1 000 cs has a large viscosity and a small *Re* that results in a large wall boundary layer thickness, which decreases the shear stress of the bubble near the wall, so the deformation from the bubble formation stage to the floating process is extremely small. However, the silicone oil with a viscosity of 100 cs has a low viscosity, a large *Re*, and a small boundary layer thickness. The bubbles are subjected to strong shear stress, so they undergo evident deformation during floating. The influence of the boundary layer causes the bubble to move along different trajectories and not just rise vertically.

Figure 14 shows the vorticity variation of bubbles near the wall and free field bubbles. The existence of the wall provides a symmetrical damage disturbance to the vortex in the flow field. According to the Kelvin circulation theorem, vortices in the flow domain can produce lateral forces. The diagram illustrates that the vortex of the fluid around the bubble in the free field is symmetrically distributed. Because the lateral force generated by the symmetrical vortex on the bubble is offset, the resultant force on the bubble is zero, which leads to no movement in the lateral direction. However, due to the presence of the wall, the flow structure around the bubble exhibits an asymmetric evolution. The reason for the difference in bubble surface velocity

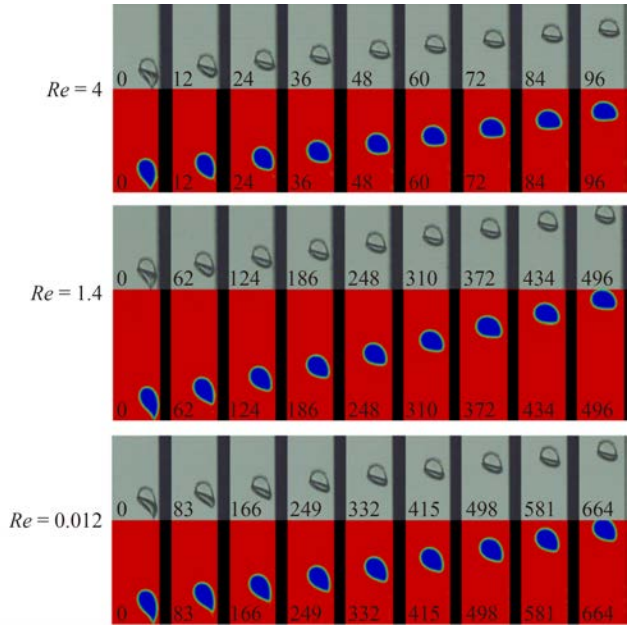

Figure 13 Comparison of initial bubble morphology changes near the wall surface in high-viscosity silicone oil

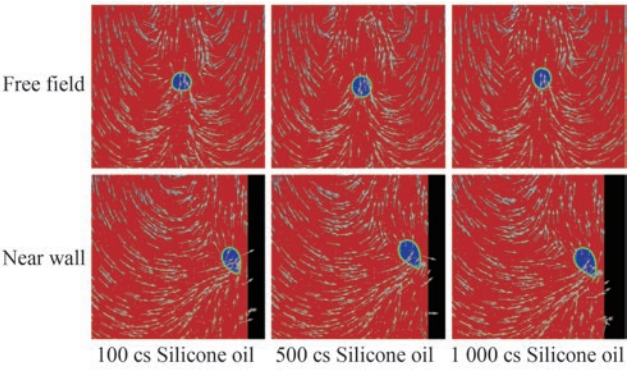

Figure 14 Flow field vorticity around the bubble

is primarily due to the boundary layer effect and the interaction between the bubble and the solid surface. When the bubble is close to the solid surface, the velocity of the fluid near the wall is influenced by viscosity, and a velocity gradient is formed. The side near the wall of the bubble surface has a lower velocity, whereas the side away from the wall is affected by the freer fluid, and the velocity is higher. This velocity difference leads to a pressure difference on the bubble surface and forms a lateral force. Therefore, the asymmetry of the flow structure provides a qualitative explanation for the attraction of bubbles due to the wall effect.

Next, six kinds of silicone oil viscosity, 1 cs (*Re* = 740), 10 cs (*Re* = 71.2), 20 cs (*Re* = 54), 100 cs (*Re* = 4), 500 cs (*Re* = 1.4), and 1 000 cs (*Re* = 0.012), are taken. Taking the centroid of the initial shape of the bubble just leaving the outlet as the coordinate origin, the displacement trajectory of the bubble during floating and the terminal velocity

map after the stable floating of the bubble are drawn.

Figure 15 shows that under the influence of the wall surface, bubbles in each viscosity of silicone oil produce lateral migration, and the lateral migration velocity decreases with viscosity increasing. The difference is that when the liquid viscosity is small, the generated bubbles have a weak interaction with the wall surface, so the wall surface has a substantial repulsive effect on the bubbles, whereas the wall surface has less attraction to the bubbles. In a period after the bubbles are generated, a faster lateral migration occurs and makes the bubbles move away from the wall surface faster. With the increase of the distance from the wall, the wall effect is weakened, and the lateral migration velocity is gradually reduced. In the high-viscosity fluid, the interaction between the bubble and the wall is strong, so the repulsive effect of the wall on the bubble is weak, the attraction is strong, and the lateral migration of the bubble is small at the beginning. When the bubble reaches a stable state and continues to rise, the lateral migration caused by the wall effect is more apparent compared with that of the low-viscosity bubble. Because the bubbles in low-viscosity silicone oil are mainly induced by the lift force of the wall surface, whereas the bubbles in high-viscosity silicone oil are mainly induced by the drag force of the wall surface, the final velocity of the bubbles in low-viscosity silicone oil is much larger than that in high-viscosity silicone oil after reaching a steady state, and as the viscosity increases, the final velocity of the bubbles decreases.

The difference is that in silicone oil with a viscosity of 1 cs because the viscosity is close to water, the bubble migration trajectory exhibits a bounce behavior similar to the wall migration in water. However, due to the different surface tension, its migration does not bounce at the wall like water but migrates away from the wall again after floating up approximately parallel to the wall within a certain distance.

4.2 Effect of the distance between the bubble and the wall on the dynamic characteristics of floating bubbles

To explore the influence of the distance between the bubble and the wall on the rising behavior of the bubble, this section uses a dimensionless parameter λ as the distance between the center of the outlet and the wall. The formula is as follows:

$$\lambda = \frac{D}{R} \tag{17}$$

where D is the actual distance from the center of the outlet to the wall, and R is the bubble radius.

With other parameters unchanged, λ = 1, 1.5, 2, 2.5, 3 silicone oil with viscosity of 100 and 1 000 cs is analyzed to explore the influence of the distance between the bubble and the wall on the floating bubble.

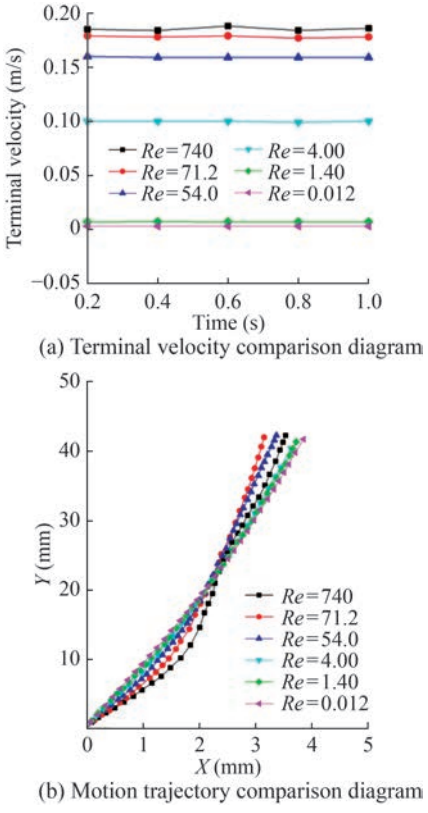

Figure 15 Comparison of bubble trajectory and terminal velocity in silicone oil with different viscosities

Figure 16 shows the initial shape changes of bubbles with different wall distances in 100 cs viscosity, and their deformations are similar. After leaving the outlet, the bottom of the bubble rises, shrinks, and gradually forms a stable state of floating. Due to the large viscosity, the bubble is subjected to evident wall-induced force when it just leaves the outlet, which results in a large deformation of the bubble shape. The deformation gradually decreases to zero with the increase of the wall distance. When the wall distance is 1 times the bubble radius, the bottom of the bubble is drawn by a noticeable wall attraction when it bounces up. However, due to the high viscosity of silicone oil, the attraction of the wall to the bubble is also greater, which hinders the contraction of the bottom; consequently, the bubble near the wall side is lower than that on the other side. With the increase of the distance from the wall, the bottom gradually becomes flat and finally forms a stable shape to float up, and the bubble size gradually decreases with the increase of the distance from the wall.

As the wall distance increases, the influence of the wall surface on the bubble gradually weakens, and the influence almost disappears when the distance is 2.5 times the bubble radius, which can be ignored.

Figure 17 shows the initial morphological changes of bubbles at different wall distances in 1 000 cs viscosity sil-

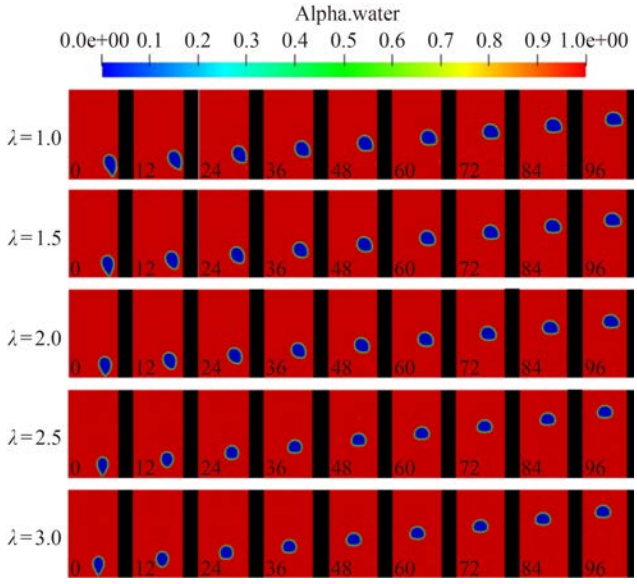

Figure 16 Comparison of initial bubble morphology at different wall distances in 100 cs viscosity silicone oil

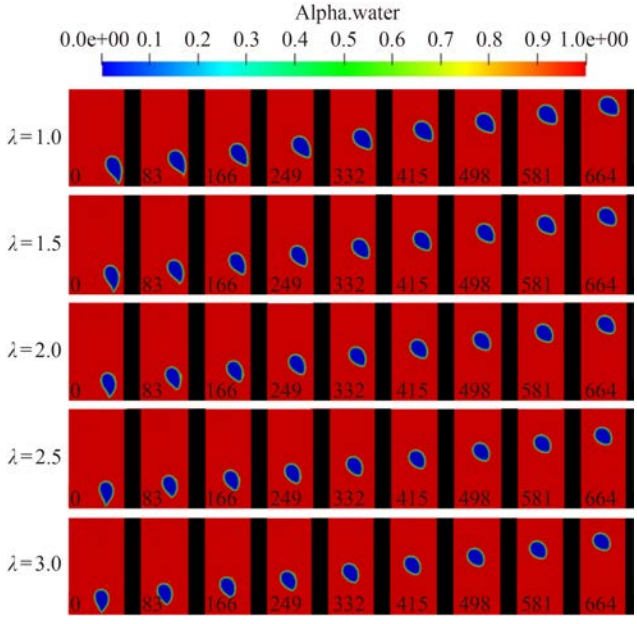

Figure 17 Comparison of initial bubble morphology at different wall distances in 1 000 cs viscosity silicone oil

icone oil. When the initial distance is 1 times the radius of the bubble, the bottom cone of the bubble undergoes large deformation during the formation stage. During the upward bounce of the bottom, the near-wall side is subjected to evident wall-induced force, which greatly affects the contraction of the bottom, and the bottom of the bubble is obviously biased toward the wall. With the further contraction of the bottom, the height difference near the wall side becomes more apparent. With the increase of the wall distance, the influence of the wall on the bubble is gradually weakened when the bubble is just out of the outlet, and the deformation is also reduced. The bubble size is also the same as that in 100 cs, which gradually decreases with the increase of wall distance. Different from 100 cs, when the wall distance is 2.5 and 3 times the bubble radius, the influence of the wall surface on the bubble shape is further reduced, but it is not reduced to almost invisible, and a certain height difference between the two sides of the bubble is observed.

Taking the same working condition as above, the centroid of the initial shape of the bubble just leaving the outlet is taken as the coordinate origin to obtain a more intuitive comparison of bubble trajectory changes. The displacement trajectory of the bubble during floating and the terminal velocity diagram of the bubble after stable floating are drawn.

Figure 18 shows the trajectory and final velocity of bubbles with different wall distances in 100 and 1 000 cs viscosity silicone oil. The movement trend of bubbles in two kinds of silicone oil is similar with different wall distances. At a close distance, the bubble is greatly affected by the wall surface, and it migrates horizontally away from the wall at a faster speed, which results in a larger lateral displacement. As the initial distance from the wall increases, the influence of the wall on the bubble gradually weakens, the lateral migration speed decreases, and its trajectory gradually approaches a straight line. With the increase of the initial wall distance, the floating terminal velocity of the bubbles in the two kinds of viscosity silicone oil becomes faster. The difference is that in 1 000 cs viscosity silicone oil, compared with 100 cs silicone oil, when the initial distance from the wall is modified, the changes in the bubble trajectory and final velocity become smaller. At close range, the bubble trajectory in 1 000 cs viscosity is closer to a straight line. At the same wall distance, the lateral migration of bubbles in 1 000 cs viscosity silicone oil is more than that in 100 cs viscosity silicone oil, but the final velocity of floating is smaller than that in 100 cs viscosity. Therefore, the wall effect in high-viscosity silicone oil decays more slowly.

4.3 Effect of gas flow rate on the dynamic characteristics of floating bubbles

To study the effect of outlet gas velocity on the bubble rising behavior near the wall, bubbles are generated at the same viscosity and the same wall distance. The surface phase velocity of the outlet gas is expressed as U_G, U_G = 0.001, 0.005, 0.01, 0.015, 0.02, in the unit of m/s, while all other parameters remain unchanged. In this section, 1 000 cs high-viscosity silicone oil is selected for analysis to explore the effect of gas flow rate on floating bubbles near the wall.

Figure 19 compares the initial morphology of bubbles near the wall with different gas flow rates in 1 000 cs viscosity silicone oil. With the increase in gas flow rate, the bubbles gradually become slender when they are separated

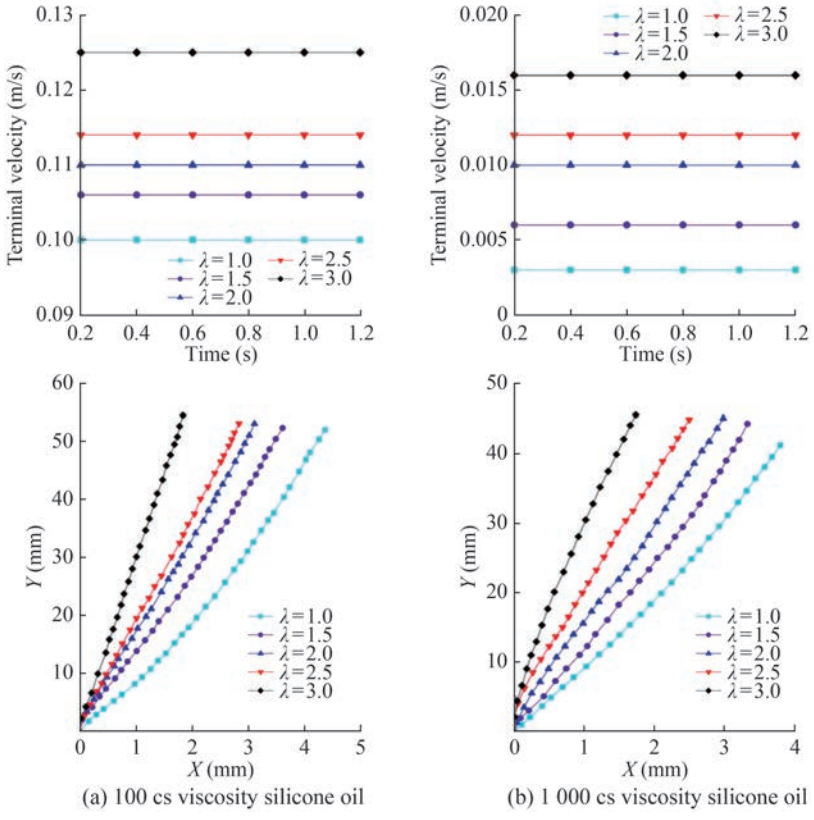

Figure 18 Comparison of bubble trajectory and terminal velocity at different wall distances

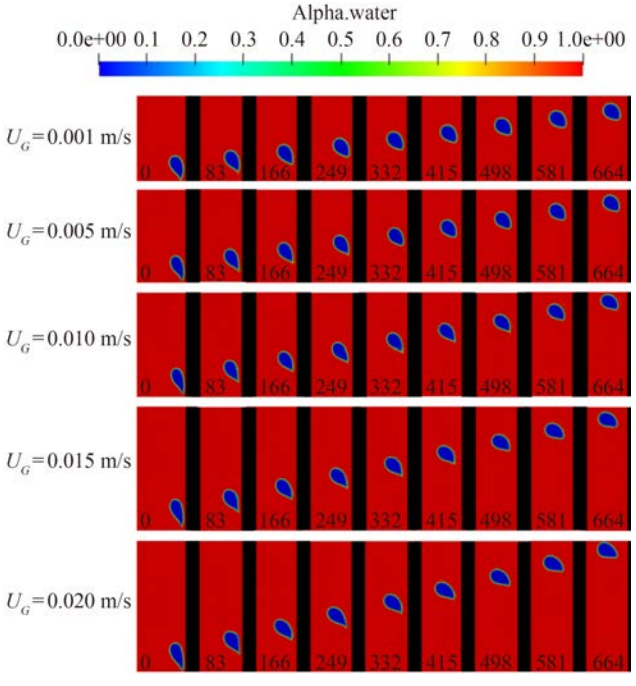

Figure 19 Comparison of initial bubble morphology of 1 000 cs silicone oil at different gas flow rates

from the outlet, and the upward rebound velocity at the bottom of the bubbles also increases so that the height difference between the top and tail of the bubbles decreases. When the gas velocity is 0.001 m/s, the bubble keeps the ellipsoid shape and rises steadily. When the gas velocity reaches 0.02 m/s, the bubble shape changes from ellipsoid to cap due to the increased gas flow rate, weakened attraction of the wall surface to the bubble, and increased influence of the buoyancy at the bottom of the bubble. Thus, the rebound velocity at the bottom increases, and the bottom of the bubble becomes flat.

Taking the same working condition as above, the centroid of the initial shape of the bubble just leaving the outlet is taken as the coordinate origin to obtain a more intuitive comparison of bubble trajectory changes. The displacement trajectory of the bubble during floating and the terminal velocity diagram of the bubble after stable floating are drawn.

Figure 20 compares the trajectory and terminal velocity of bubbles on the wall with different gas flow rates in 1 000 cs viscosity silicone oil. With the increase of gas flow rate, the terminal velocity of the bubble rising also increases. The trajectory diagram reveals that as the gas flow rate increases, the bubble moves faster in the vertical direction because the initial velocity of the bubble when it leaves the outlet increases. The lateral displacement slows down as the flow rate increases. The initial vertical upward velocity increases first, and after a distance from the wall, the velocity decreases and stabilizes.

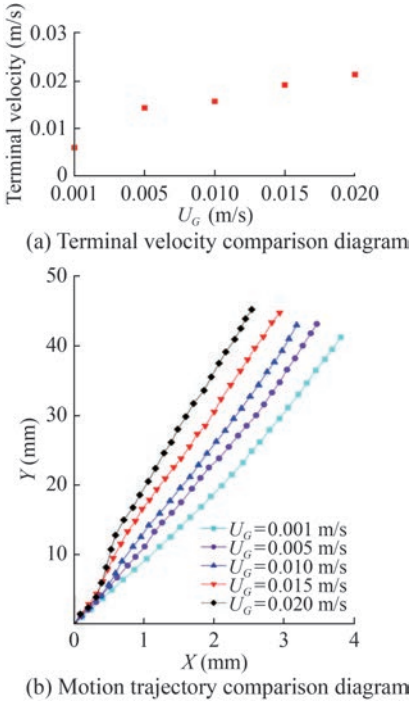

Figure 20 Comparison of trajectory and terminal velocity of bubbles with different gas flow rates in 1 000 cs silicone oil

5 Conclusions

A numerical model of small-scale bubbles on the orifice wall is established based on the VOF method in OpenFOAM, and its numerical accuracy is verified by model experiments. On this basis, the constitutive relations of different fluid media are considered, and the dynamic characteristics of bubbles floating near the wall under the influence of the viscosity effect are mainly explored. The conclusions are summarized as follows:

1) Compared with the bubble in the unbounded flow field, the force of the bubble near the wall is more complex, which includes fluid resistance and wall-induced force. Under the influence of the wall, the bubble migrates from the vertical rigid boundary, and the lateral migration speed decreases as the bubble continues to rise.

2) The characteristics of induced force in the longitudinal direction of the wall are closely related to the change in liquid viscosity. Induced lift is the main form of action under low-viscosity conditions, and induced resistance is the main form under high-viscosity conditions. As the viscosity increases, the bubble terminal velocity decreases, so the effect of high-viscosity liquid is slower than that of low viscosity. As the initial wall distance increases, the effect of the wall on the bubble gradually weakens.

3) In high-viscosity liquid, with the increase of outlet gas velocity, the terminal velocity of the rising bubble also increases, and the vertical displacement of the bubble is faster. The lateral displacement slows down as the flow rate increases. The initial vertical upward velocity increases first, and after a distance from the wall, the velocity decreases and stabilizes.

4) As the liquid viscosity increases, the *Re* of bubbles gradually decreases and reaches a minimum of 0.012, which is similar to that of micron-sized bubbles in the water. Therefore, the dynamic evolution mechanism of small-scale bubbles in different fluid media in this paper can provide an effective reference for industrial production, drag reduction, and ultrasonic cleaning.

Funding Supported by the National Natural Science Foundation of China (Grant No. 52271319), the Jiangsu Funding Program for Excellent Postdoctoral Talent, and the Postdoctoral Fellowship Program of China Postdoctoral Science Foundation (Grant No. GZC20240618), the Natural Science Foundation of Jiangsu Province of China (BK20231525).

Competing interest The authors have no competing interests to declare that are relevant to the content of this article.

References

Amaya-Bower L, Lee T (2010) Single bubble rising dynamics for moderate Reynolds number using Lattice Boltzmann Method. Computers and Fluids 39(7): 1191-1207. DOI: 10.1016/j.compfluid.2010.03.003

Corchero G, Medina A, Higuera FJ (2006) Effect of wetting conditions and flow rate on bubble formation at orifices submerged in water. Colloids & Surfaces A Physicochemical & Engineering Aspects 90(1-3): 41-49. DOI: 10.1016/j.colsurfa.2006.04.046

Debisschop KM, Miksis MJ, Eckmann DM (2000) Bubble rising in an inclined channel. Physics of Fluids 14(1): 93-106. DOI: 10.1007/978-94-017-1996-4_15

Gan N, Yao XL, Su B (2022) Study on the dynamic behaviors of a near wall ventilated bubble using OpenFOAM. Ocean Engineering 257: 111650. DOI: 10.1016/J.OCEANENG.2022.111650

Gong Z, Cai J, Lu Q (2020) Experiment characterization of the influence of wall wettability and inclination angle on bubble rising process using PIV. European Journal of Mechanics-B/Fluids 81(1): 62-75. DOI: 10.1016/j.euromechflu.2020.01.005

Jeong H, Park H (2015) Near-wall rising behaviour of a deformable bubble at high Reynolds number. Journal of Fluid Mechanics 771: 564-594. DOI: 10.1017/jfm.2015.191

Mundhra R, Lakkaraju R, Das KP (2023) Effect of wall proximity and surface tension on a single bubble rising near a vertical wall. Water 15(8): 1567. DOI: 10.3390/W15081567

Naseer HU, Ahmed Z, Izbassarov D (2023) Dynamics and interactions of parallel bubbles rising in a viscoelastic fluid under buoyancy. SSRN Electronic Journal 313: 105000. DOI: 10.2139/ssrn.4147495

Premlata AR, Tripathi MK, Sahu KC (2015) Dynamics of rising bubble inside a viscosity-stratified medium. Physics of Fluids 27(7): 072105-072105. DOI:10.1063/1.4927521

Rozario A, Viswanathan NN, Basu S (2018) Rise of gas bubbles across the interface between two liquids. Metallurgical and Materials Transactions B 50(1): 31-56. DOI: 10.1007/s11663-018-1434-1

Shi P, Tholan V, Sommer AE (2023) Forces on a nearly spherical bubble rising in an inclined channel flow. International Journal of Multiphase Flow 169: 126-140. DOI: 10.1016/j.ijmultiphaseflow.2023.104620

Snabre P, Magnifotcham F (1998) I. Formation and rise of a bubble stream in a viscous liquid. European Physical Journal B Condensed Matter & Complex Systems 4(3): 369-377. DOI: 10.1007/s100510050392

Sugiyama K, Takemura F (2010) On the lateral migration of a slightly deformed bubble rising near a vertical plane wall. Journal of Fluid Mechanics 662: 209-231. DOI: 10.1017/S0022112010003149

Takemura F, Magnaudet J (2003) The transverse force on clean and contaminated bubbles rising near a vertical wall at moderate Reynolds number. Journal of Fluid Mechanics 495: 235-253. DOI: 10.1017/S0022112003006232

Takemura F, Takagi S, Magnaudet J (2002) Drag and lift forces on a bubble rising near a vertical wall in a viscous liquid. J. Fluid Mech 461: 277-300. DOI: 10.1017/S0022112002008388

Tian Z, Cheng YW, Li X (2019) Bubble shape and rising velocity in viscous liquids at high temperature and pressure. Experimental Thermal & Fluid Science 102: 528-538. DOI: 10.1016/j.expthermflusci.2018.12.018

Xu Y, Yang G, Hu D (2023) A three-dimensional ISPH-FVM coupling method for simulation of bubble rising in viscous stagnant liquid. Ocean engineering 278: 114477. DOI: 10.1016/j.oceaneng.2023.114497

Yan HJ, Zhang HY, Zhang HM (2023) Three-dimensional dynamics of a single bubble rising near a vertical wall: Paths and wakes. Petroleum Science 20(3): 1874-1884. DOI: 10.1016/j.petsci.2023.02.014

Zhang AM, Li SM, Xu RZ (2024) A theoretical model for compressible bubble dynamics considering phase transition and migration. Journal of Fluid Mechanics 999(458): A58-A58. DOI: 10.1017/JFM.2024.954

Zhang L, Yang C, Mao ZS (2008) Unsteady motion of a single bubble in highly viscous liquid and empirical correlation of drag coefficient. Chemical Engineering Science 63(8): 2099-2106. DOI: 10.1016/j.ces.2008.01.010

Zheng LY, Zhang B, Luo Y (2023) Mass transfer dynamics of single CO_2 bubbles rising in monoethanolamine solutions: Experimental study and mathematical model. Chemical Engineering Journal 465: 142761. DOI:10.1016/J.CEJ.2023.142761